

High speed plasmonic modulator array enabling dense optical interconnect solutions

W. Heni,^{1,4,5} C. Hoessbacher,^{1,4,6} C. Haffner,¹ Y. Fedoryshyn,¹ B. Baeuerle,¹ A. Josten,¹
D. Hillerkuss,¹ Y. Salamin,¹ R. Bonjour,¹ A. Melikyan,² M. Kohl,² D. L. Elder,³
L. R. Dalton,³ C. Hafner,¹ and J. Leuthold^{1,7}

¹*Institute of Electromagnetic Fields (IEF), ETH Zurich, 8092 Zurich, Switzerland*

²*Institute of Microstructure Technology (IMT), Karlsruhe Institute of Technology (KIT), 76131 Karlsruhe, Germany*

³*Department of Chemistry, University of Washington, Seattle, WA 98195-1700, USA*

⁴*contributed equally*

⁵*wheni@ethz.ch*

⁶*choessbacher@ethz.ch*

⁷*juergleuthold@ethz.ch*

Abstract: Plasmonic modulators might pave the way for a new generation of compact low-power high-speed optoelectronic devices. We introduce an extremely compact transmitter based on plasmonic Mach-Zehnder modulators offering a capacity of 4×36 Gbit/s on a footprint that is only limited by the size of the high-speed contact pads. The transmitter array is contacted through a multicore fiber with a channel spacing of 50 μm .

©2015 Optical Society of America

OCIS codes: (250.5403) Plasmonics; (230.2090) Electro-optical devices; (250.4110) Modulators; (200.4650) Optical interconnects.

References and links

1. D. A. Miller, "Physical reasons for optical interconnection," *Int. J. Optoelectron.* **11**, 155–168 (1997).
2. Z. Li, I. Shubin, and X. Zhou, "Optical interconnects: recent advances and future challenges," *Opt. Express* **23**(3), 3717–3720 (2015).
3. G. Denoyer, C. Cole, A. Santipo, R. Russo, C. Robinson, L. Li, Y. Zhou, J. A. Chen, B. Park, F. Boeuf, S. Crémer, and N. Vulliet, "Hybrid silicon photonic circuits and transceiver for 50 Gb/s NRZ transmission over single-mode fiber," *J. Lightwave Technol.* **33**(6), 1247–1254 (2015).
4. R. Dangel, J. Hofrichter, F. Horst, D. Jubin, A. La Porta, N. Meier, I. M. Soganci, J. Weiss, and B. J. Offrein, "Polymer waveguides for electro-optical integration in data centers and high-performance computers," *Opt. Express* **23**(4), 4736–4750 (2015).
5. V. I. Kopp, J. Park, M. Wlodawski, E. Hubner, J. Singer, D. Neugroschl, A. Z. Genack, P. Dumon, J. Van Campenhout, and P. Absil, "Two-dimensional, 37-channel, high-bandwidth, ultra-dense silicon photonics optical interface," *J. Lightwave Technol.* **33**(3), 653–656 (2015).
6. L. Schares, J. A. Kash, F. E. Doany, C. L. Schow, C. Schuster, D. M. Kuchta, P. K. Pepeljugoski, J. M. Trehwella, C. W. Baks, R. A. John, S. Lei, Y. H. Kwark, R. A. Budd, P. Chiniwalla, F. R. Libsch, J. Rosner, C. K. Tsang, G. S. Patel, J. D. Schaub, R. Dangel, F. Horst, B. J. Offrein, D. Kucharski, D. Guckenberger, S. Hegde, H. Nyikal, L. Chao-Kun, A. Tandon, G. R. Trott, M. Nystrom, D. P. Bour, M. R. T. Tan, and D. W. Dolfi, "Terabus: Terabit/second-class card-level optical interconnect technologies," *IEEE J. Sel. Top. Quantum Electron.* **12**(5), 1032–1044 (2006).
7. J. Ferrara, W. Yang, L. Zhu, P. Qiao, and C. J. Chang-Hasnain, "Heterogeneously integrated long-wavelength VCSEL using silicon high contrast grating on an SOI substrate," *Opt. Express* **23**(3), 2512–2523 (2015).
8. H. Subbaraman, X. Xu, A. Hosseini, X. Zhang, Y. Zhang, D. Kwong, and R. T. Chen, "Recent advances in silicon-based passive and active optical interconnects," *Opt. Express* **23**(3), 2487–2510 (2015).
9. G. T. Reed, G. Mashanovich, F. Y. Gardes, and D. J. Thomson, "Silicon optical modulators," *Nat. Photonics* **4**(8), 518–526 (2010).
10. M. L. Brongersma and V. M. Shalaev, "Applied physics. The case for plasmonics," *Science* **328**(5977), 440–441 (2010).
11. J. Leuthold, C. Hoessbacher, S. Muehlbrandt, A. Melikyan, M. Kohl, C. Koos, W. Freude, V. Dolores-Calzadilla, M. Smit, I. Suarez, J. Martínez-Pastor, E. P. Fitrakis, and I. Tomkos, "Plasmonic communications: light on a wire," *Opt. Photonics News* **24**(5), 28–35 (2013).
12. K. Liu, C. R. Ye, S. Khan, and V. J. Sorger, "Review and perspective on ultrafast wavelength-size electro-optic modulators," *Laser Photonics Rev.* **9**(2), 172–194 (2015).

13. A. Emboras, C. Hoessbacher, C. Haffner, W. Heni, U. Koch, P. Ma, Y. Fedoryshyn, J. Niegemann, C. Hafner, and J. Leuthold, "Electrically controlled plasmonic switches and modulators," *IEEE J. Sel. Top. Quantum Electron.* **21**(4), 276 (2015).
14. C. Haffner, W. Heni, Y. Fedoryshyn, J. Niegemann, A. Melikyan, D. L. Elder, B. Baeuerle, Y. Salamin, A. Josten, U. Koch, C. Hoessbacher, F. Ducry, L. Juchli, A. Emboras, D. Hillerkuss, M. Kohl, L. R. Dalton, C. Hafner, and J. Leuthold, "All-plasmonic Mach-Zehnder modulator enabling optical high-speed communication at the microscale," *Nat. Photonics* **9**(8), 525–528 (2015).
15. A. Melikyan, L. Alloatti, A. Muslija, D. Hillerkuss, P. C. Schindler, J. Li, R. Palmer, D. Korn, S. Muehlbrandt, D. Van Thourhout, B. Chen, R. Dinu, M. Sommer, C. Koos, M. Kohl, W. Freude, and J. Leuthold, "High-speed plasmonic phase modulators," *Nat. Photonics* **8**(3), 229–233 (2014).
16. W. Heni, C. Haffner, B. Baeuerle, Y. Fedoryshyn, A. Josten, D. Hillerkuss, J. Niegemann, A. Melikyan, M. Kohl, D. L. Elder, L. R. Dalton, C. Hafner, and J. Leuthold, "108 Gbit/s plasmonic Mach-Zehnder modulator with > 70 GHz electrical bandwidth," *J. Lightwave Technol.* in press (2015).
17. C. Hoessbacher, W. Heni, A. Melikyan, Y. Fedoryshyn, C. Haffner, B. Baeuerle, A. Josten, D. Hillerkuss, Y. Salamin, M. Kohl, D. Elder, L. Dalton, C. Hafner, and J. Leuthold, "Dense plasmonic Mach-Zehnder modulator array for high-speed optical interconnects," in *Advanced Photonics 2015* (Optical Society of America, 2015), paper IM2B.1.
18. J. Leuthold, C. Haffner, W. Heni, C. Hoessbacher, J. Niegemann, Y. Fedoryshyn, A. Emboras, C. Hafner, A. Melikyan, M. Kohl, D. L. Elder, and L. R. Dalton, "Plasmonic modulators and switches" in *Surface Plasmon Photonics* (SPP, 2015).
19. M. W. Knight, H. Sobhani, P. Nordlander, and N. J. Halas, "Photodetection with active optical antennas," *Science* **332**(6030), 702–704 (2011).
20. S. Muehlbrandt, A. Melikyan, K. Köhnle, T. Harter, A. Muslija, P. Vincze, S. Wolf, P. Jakobs, Y. Fedoryshyn, W. Freude, J. Leuthold, C. Koos, and M. Kohl, "Plasmonic internal photoemission detectors with responsivities above 0.12 A/W," in *CLEO: 2015* (Optical Society of America, 2015), pp. FTh3E.3.
21. N. Dupuis, B. Lee, J. E. Proesel, A. Rylyakov, R. Rimolo-Donadio, C. Baks, C. L. Schow, A. Ramaswamy, J. E. Roth, and R. Guzzon, "30Gbps optical link utilizing heterogeneously integrated III-V/Si photonics and CMOS circuits," in *OFC 2014* (IEEE, 2014), pp. 1–3.
22. E. Timurdogan, Z. Su, K. Settaluri, S. Lin, S. Moazeni, C. Sun, G. Leake, D. D. Coolbaugh, B. Moss, M. Moresco, V. Stojanovi, and M. R. Watts, "An ultra low power 3D integrated intra-chip silicon electronic-photonics link," in *OFC 2015* (Optical Society of America, March 2015), pp. Th5B.8.
23. A. Ramaswamy, J. Roth, E. Norberg, R. S. Guzzon, J. Shin, J. Imamura, B. Koch, D. Sparacin, G. Fish, and B. G. Lee, "A WDM 4x28Gbps integrated silicon photonic transmitter driven by 32nm CMOS driver ICs," in *OFC 2015* (Optical Society of America, 2015), pp. Th5B.5.
24. A. Melikyan, K. Köhnle, M. Lauermann, R. Palmer, S. Koeber, S. Muehlbrandt, P. C. Schindler, D. L. Elder, S. Wolf, W. Heni, C. Haffner, Y. Fedoryshyn, D. Hillerkuss, M. Sommer, L. R. Dalton, D. Van Thourhout, W. Freude, M. Kohl, J. Leuthold, and C. Koos, "Plasmonic-organic hybrid (POH) modulators for OOK and BPSK signaling at 40 Gbit/s," *Opt. Express* **23**(8), 9938–9946 (2015).
25. R. W. Boyd, *Nonlinear Optics* (Academic, 2003).
26. J. J. Wolff and R. Wortmann, "Organic materials for second-order non-linear optics," *Adv. Phys. Org. Chem.* **32**, 121–217 (1999).
27. D. M. Burland, R. D. Miller, and C. A. Walsh, "Second-order nonlinearity in poled-polymer systems," *Chem. Rev.* **94**(1), 31–75 (1994).
28. L. R. Dalton, P. A. Sullivan, and D. H. Bale, "Electric field poled organic electro-optic materials: state of the art and future prospects," *Chem. Rev.* **110**(1), 25–55 (2010).
29. J. Leuthold, C. Koos, W. Freude, L. Alloatti, R. Palmer, D. Korn, J. Pfeifle, M. Lauermann, R. Dinu, S. Wehrli, M. Jazbinsek, P. Gunter, M. Waldow, T. Wahlbrink, J. Bolten, H. Kurz, M. Fournier, J.-M. Fedeli, H. Yu, and W. Bogaerts, "Silicon-organic hybrid electro-optical devices," *IEEE J. Sel. Top. Quantum Electron.* **19**(6), 114–126 (2013).
30. D. L. Elder, S. J. Benight, J. Song, B. H. Robinson, and L. R. Dalton, "Matrix-assisted poling of monolithic bridge-disubstituted organic NLO chromophores," *Chem. Mater.* **26**(2), 872–874 (2014).
31. S. Koeber, R. Palmer, M. Lauermann, W. Heni, D. L. Elder, D. Korn, M. Woessner, L. Alloatti, S. Koenig, P. C. Schindler, H. Yu, W. Bogaerts, L. R. Dalton, W. Freude, J. Leuthold, and C. Koos, "Femtojoule electro-optic modulation using a silicon-organic hybrid device," *Light Sci. Appl.* **4**(2), e255 (2015).
32. L. R. Dalton, "Rational design of organic electro-optic materials," *J. Phys. Condens. Mat.* **15**(20), R897–R934 (2003).
33. L. R. Dalton, D. Lao, B. C. Olbricht, S. Benight, D. H. Bale, J. A. Davies, T. Ewy, S. R. Hammond, and P. A. Sullivan, "Theory-inspired development of new nonlinear optical materials and their integration into silicon photonic circuits and devices," *Opt. Mater.* **32**(6), 658–668 (2010).
34. Y. Shi, L. Yan, and A. E. Willner, "High-speed electrooptic modulator characterization using optical spectrum analysis," *J. Lightwave Technol.* **21**(10), 2358–2367 (2003).
35. F. Chang, K. Onohara, and T. Mizuoichi, "Forward error correction for 100 G transport networks," *IEEE Commun. Mag.* **48**(3), S48–S55 (2010).

1. Introduction

High-speed optical interconnects are gradually replacing electrical solutions [1]. To satisfy the ever growing bandwidth requirements, they must offer highest speed at lowest power consumption with the smallest possible footprint [2].

Optical interconnect solutions must overcome three fundamental challenges: First, they need transmitters that can be arranged in a highly parallel manner; second, they need a fiber-to-chip interface to overcome distances from millimeters up to hundreds of meters; last, they need highly parallel and compact detector solutions. Among these three challenges, the detector issues have indeed been addressed convincingly in the last years. Today, there are extremely compact detector arrays for direct and coherent detection e.g. in the form of integrated silicon-germanium detectors that offer operation beyond 56 Gbit/s [3]. As a fiber-to-chip interface, fiber ribbons and plastic interconnect solutions are frequently used. However, the typical spacing of ribbons (125 μm) does not allow particular dense integration, and, furthermore, plastic interconnects are mostly a solution only for short distances [4]. Alternatively, multicore fibers (MCF) that are matched to out-of-plane surface couplers provide both, a relatively dense optical interface [5] and transmission over long distances. The biggest challenge though, remains a most dense integration of transmitters. Besides approaches based on direct modulation of VCSELs [6, 7], silicon photonics offers a variety of paths for combining an external laser source and on-chip modulators [8, 9]. However, silicon photonic modulators occupy a length in the order of several millimeters, if not incorporated into a resonant structure. More recently, plasmonics has emerged as an interesting and compact solution for integration of active devices [10, 11]. Plasmonics indeed allows for extremely compact devices of a few μm^2 , because – in contrast to photonic waves – surface plasmon polaritons (SPPs) are not diffraction limited [12, 13]. Moreover, plasmonics offers high speed [14, 15], line rates above 100 Gbit/s [16] and devices can be manufactured using large-scale production techniques of the electronics industry.

In this paper, we introduce a new optical interconnect solution relying on a plasmonic Mach-Zehnder modulator (MZM) array. A multicore fiber (MCF) with a 50 μm channel spacing connects the array. The transmitter is demonstrated to operate at 4×36 Gbit/s. The array has been characterized for optical interchannel crosstalk which was found to be below -31 dB. No electrical crosstalk was observed. The MZMs showed no bandwidth limitation up to 70 GHz. The individual MZMs comprise plasmonic phase modulator sections that are as short as 12.5 μm . This allows for a dense arrangement of the MZMs that is only limited by the size of the contact pads needed for addressing the devices with electrical probes. The devices are able to operate over a broad spectral range of >100 nm. Application scenarios include both space division (SDM) and wavelength division multiplexing (WDM) applications. This is because each core of the MCF can be addressed individually. The invited paper is based on work published in [14, 17, 18].

2. Optical interconnect solution

The interconnect solution envisioned here is made possible by dense plasmonic modulator arrays. Such plasmonic modulators can be integrated with plasmonic detectors (e.g [19, 20].), conventional detectors that are extremely compact as well and with electronics [3, 21–23], making them attractive transceivers for data center applications. Figure 1 illustrates two operation scenarios, with space-division multiplexing (SDM), Fig. 1(a), or wavelength-division multiplexing (WDM), Fig. 1(b). In both scenarios, light of centralized lasers is distributed via a switch and MCFs to the integrated transceivers. The same MCFs also

provide connection for optical input and output signals of the transceivers. They couple light to matched on-chip grating coupler (GC) arrays.

In the SDM application scenario, Fig. 1(a), the transmitter (Tx) is fed by a single laser source. The laser signal is then split on chip, fed to four modulators and is encoded with information. Each signal is sent back through a different core of the MCF. The modulated signals are fed to a central switch from where they are distributed to remote locations and receivers (Rx). In the Rx, the signals are received in a direct or coherent detection scheme using the LO. The receiver may be integrated together with the plasmonic modulators on the same chip, e.g. in form of extremely compact plasmonic detectors [19, 20] or germanium waveguide detectors [3]. In the WDM scheme, Fig. 1(b), the interconnect is fed by external lasers emitting a set of wavelengths, four in this example ($\lambda_1 \dots \lambda_4$). The transmitter consists of a modulator array followed by integrated or external multiplexers (MUX). At the receiver, a demultiplexer separates and individually detects the wavelength channels.

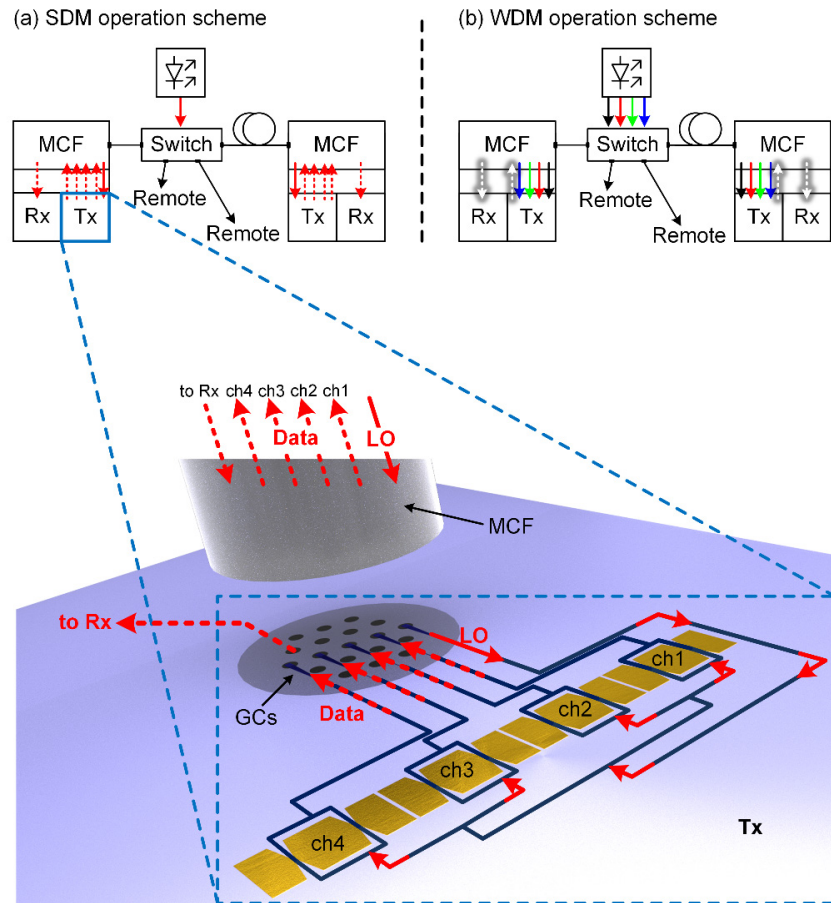


Fig. 1. (a) Space division multiplexing scheme with blow-up of the compact plasmonic transmitter (Tx) for high-speed optical interconnects in data center applications. The interconnect is fed by a central laser source, while a switching network distributes the signals. The central laser signal (LO, solid line) is inter-connected by a multicore fiber (MCF) to the integrated plasmonic Tx via grating couplers (GCs). The Tx splits the laser into four channels and sends each signal to a modulator, so that several data streams each are encoded. The individual signals are then sent back through different cores of the MCF (dashed lines). Finally, the modulated signals are distributed by the switch to the receivers (Rx) which may be realized on the same chip as the Tx. (b) Wavelength division multiplexing scheme where the MCF carries laser light of different wavelengths that may be multiplexed on chip or externally.

3. Plasmonic Mach-Zehnder modulators

In this paper we chose plasmonic Mach-Zehnder modulator (MZM) configurations to encode information onto an optical carrier [16, 24]. We start this section by first detailing the operation principle of the plasmonic phase modulators (PPMs) [15] in section 3.1 and then discussing the MZM configuration and its performance.

3.1 Plasmonic-Organic Hybrid (POH) phase modulators

Phase modulators in the plasmonic-organic hybrid (POH) approach exploit the large nonlinearity of an organic nonlinear optical (NLO) material for efficient switching. They are formed of a plasmonic metal-insulator-metal (MIM) slot waveguide to guide the light, where the slot is filled with a second-order NLO material, see Fig. 2(a). In the inset of Fig. 2(b), it can be seen how the plasmonic mode is well confined to the slot. The metallic structures of the MIM waveguide not only confine the plasmonic mode but also serve as electrical contacts to encode the information. When a voltage is applied to the electrodes, it will drop off across the narrow slot and the refractive index in the slot will change due to the linear electro-optic effect. The advantage of plasmonic phase modulators over diffraction limited optical counterparts is best seen from Fig. 2(b). Figure 2(b) shows the enormous effective refractive index change Δn_{eff} experienced by a plasmonic MIM mode when the slot width decreases for a given driving voltage of $U_d = 3$ V. The simulation parameters for Fig. 2(b) are according to [14].

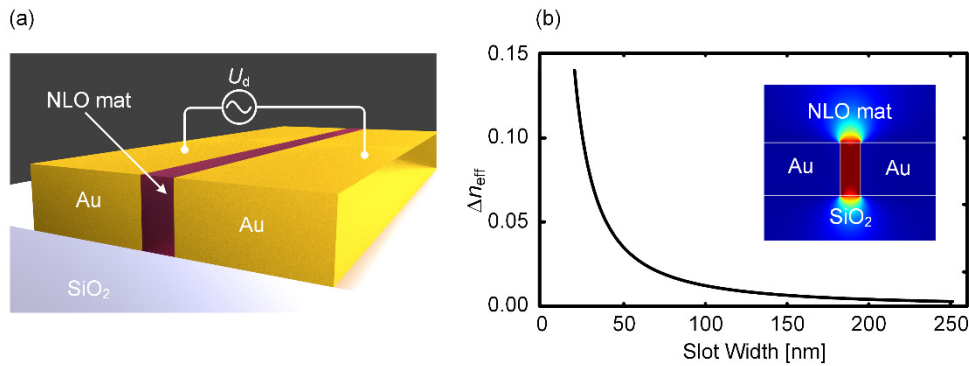


Fig. 2. (a) The plasmonic-organic hybrid (POH) phase modulator consists of two gold (Au) electrodes being separated by a narrow slot to form the plasmonic MIM waveguide. The slot is filled with an organic NLO material to exploit the Pockels effect. (b) Effective refractive index change in the plasmonic phase modulator as a function of the MIM slot width, when the driving voltage is fixed to 3 V. It can be seen that Δn_{eff} increases strongly for narrower plasmonic slots due to a high field interaction factor Γ , because of $\Delta n_{\text{mat}} \propto 1/w_{\text{slot}}$ and due to an increase of the slowdown of the energy velocity with decreasing slot width. The inset shows the corresponding mode profile at $w_{\text{slow}} = 75$ nm, gold height $h_{\text{Au}} = 200$ nm. Adapted from [14].

The origin of this strong change of n_{eff} for narrow plasmonic slot waveguides have been discussed in more detail in [14]. It can be attributed to three factors as follows:

$$\Delta n_{\text{eff}} = \Gamma \frac{\Delta n_{\text{mat}}}{n_{\text{mat}}} n_{\text{slow}}. \quad (1)$$

First, the field energy interaction factor Γ of the plasmonic MIM mode is large. It describes the ratio of the field energy of the slot mode along the active axis of the nonlinear material to

the total energy of the mode. The field energy interaction factor Γ is a useful number as only the electric field energy in the slot that is polarized in the direction of the active axis of the NLO material will experience nonlinear interaction. For a slot width of 75 nm it can exceed a value of 0.5 – and thus is four times larger than for a more conventional silicon slot waveguide. Second, the surface-plasmon polariton dispersion leads to a slowdown factor n_{slow} . As an example, for a 75 nm slot width Δn_{eff} is enhanced by a slowdown factor of $n_{\text{slow}} = 3.5$. Third, the electro-optic activity of the NLO material induces a refractive index change Δn_{mat} . This change is described by the Pockels effect [25]. The Pockels effect leads to a linear change of the refractive index depending on a static or low frequency field U_d / w_{slot} (drive voltage U_d , slot width w_{slot}) and the electro-optic coefficient r_{33} of the material

$$\Delta n_{\text{mat}} = -\frac{r_{33}}{2} n_{\text{mat}}^3 \frac{U_d}{w_{\text{slot}}}. \quad (2)$$

It can be seen, how the refractive index change increases when the slot width is decreased. When decreasing the slot width from 150 nm to 50 nm, for example, one can win a factor three in efficiency. A high r_{33} is essential for high modulation efficiencies, though. Since after deposition of the NLO material the dipolar chromophores are randomly oriented (no r_{33}), the nonlinear molecules have to be aligned in a non-centrosymmetric order [26]. This can be achieved by electric-field poling of the material [27, 28]. Electric-field poling is performed by applying an electric field while heating the material to its glass-transition temperature. The molecules align parallel to the applied field and thereby the nonlinearity r_{33} is induced.

Moreover, another factor two has been won by realizing the device as an unterminated open circuit [29]. This gives a factor two advantage over a terminated traveling waveguide approach, since twice the incident voltage drops across the device. The traveling wave approach is not needed here as the device is ultra-compact so that the back-reflected wave does not degrade the performance.

In conclusion, the approach takes advantage of at least four factors that in combination lead to a remarkably short device. The four factors are the large energy interaction factor Γ , the enhancement due to the plasmonic slow-down by n_{slow} , the large relative refractive index change $\Delta n_{\text{mat}} / n_{\text{mat}}$ which is due to a choice of a material with a large Pockels effect but also due to an inverse proportional increase when reducing the slot width, and last, an open-circuit operation. All of which allows us to fabricate the phase modulators with lengths of a few micrometers. The very short lengths of the modulators offset plasmonic losses.

3.2 Photonic Mach-Zehnder interferometer

The previously described POH phase modulators are integrated into a silicon photonic Mach-Zehnder interferometer for amplitude modulation. The arrangement of the phase-shifters in an MZM configuration not only allows operation in the push-pull mode with half the peak-voltage but also provides an almost ideal amplitude transfer function. In this paper we have chosen a hybrid approach, where all the passive waveguides are implemented as silicon waveguides and only the active phase-modulator sections are fabricated as plasmonic waveguides. An advantage of this approach is that most components are based on an established and reliable low-loss silicon-on-insulator technology, while plasmonics is only introduced where confinement and speed is crucial.

The structure of the plasmonic MZM is depicted in Fig. 3. The modulator consists of a silicon Mach-Zehnder interferometer (MZI) with PPMs in each arm. Light is coupled to the chip using fiber-to-chip grating couplers and is fed to the MZI by single mode silicon waveguides. Multimode interference (MMI) couplers are used to split the light onto the two arms of the MZI. After the phase modulator section, the two arms of the MZI are combined

using once more an MMI. Interference in the MMI translates the phase modulation induced in the two arms into an amplitude modulation.

The modulator is electrically contacted by ground-signal-ground (GSG) RF probes, see Fig. 3. The metals of the plasmonic MIM waveguides also serve as the contact pads of the modulator. This way, the RF probe is directly contacted to the plasmonic waveguide which makes RC time constants small. The driving voltage drops off across the two slots. As can be seen in Fig. 3, poling direction (red arrows) and direction of the driving field (blue arrows) are opposed in one arm and aligned in the other one. This allows to operate the device in the so-called “push-pull” operation mode, where opposite phase shifts are induced in the two PPMs upon applying a signal at the center electrode. The corresponding amplitude transfer function is given in the ideal case by [16]

$$\frac{E_{\text{out}}(U_d)}{E_{\text{in}}} \propto \cos\left(\frac{2\pi}{\lambda_{\text{OC}}}\Delta n_{\text{eff}}(U_d)L - \Phi_{\text{bias}}\right), \quad (3)$$

where E_{in} is the optical electric field sent into the modulator, λ_{OC} the wavelength of the optical carrier, L is the length of PPMs and E_{out} is the optical electric field at the modulator output. The latter follows a cosine function and varies with Δn_{eff} , that in turn depends linearly on the driving voltage U_d . The operation point of the modulator can be adjusted by a phase offset Φ_{bias} , either by applying a bias DC voltage or by adjusting the wavelength in case of an imbalanced MZI.

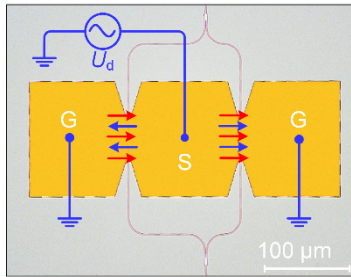


Fig. 3. Mach-Zehnder modulator (MZM) in push-pull operation: Two plasmonic phase modulators (PPMs) are arranged in an imbalanced MZI configuration with silicon multimode interference (MMI) couplers as splitters and combiners. The MZM comprises ground-signal-ground (GSG) electrodes. When an electrical signal is applied to the S electrode, the voltage drops across the plasmonic MIM waveguides, blue arrows. In this operation mode, the electrical driving and the poling field (red arrows) directions are aligned in the phase modulator of one MZM arm, but have opposite signs in the other phase modulator. Therefore, opposite refractive index changes are induced in the two respective phase modulators. The MZM is operated in push-pull operation. Adapted from [16].

4. Dense integration - plasmonic Mach-Zehnder modulator arrays

4.1 Design and fabrication

We have fabricated an array of four silicon-plasmonic-organic hybrid MZMs. A microscope image of the MZM array is depicted in Fig. 4. The key elements are 12.5 μm long PPMs. They are formed by two gold (Au) electrodes separated by a 75 nm wide slot. For direct electrical probing with standard 100 μm pitched ground-signal-ground (GSG) probes we increased the distance between MZMs to 300 μm . However, the actual footprint required by the devices is only a few tens of μm^2 . This leaves ample room for scaling down once electronics and photonics are cointegrated. The optical interface consists of GCs with a 50 μm spacing and is matched to the channel spacing of the multicore fiber (MCF) [5].



Fig. 4. Optical microscope image of the fabricated four-channel MZM array contacted by RF probes. The plasmonic phase modulators are $12.5 \mu\text{m}$ long with slot widths of 75 nm .

The MZM array was produced in-house on a silicon-on-insulator (SOI) wafer. E-beam lithography in combination with dry-etching was applied to pattern the photonic components, namely the Si waveguides ($h_{\text{Si}} = 220 \text{ nm}$, $w = 450 \text{ nm}$), MMIs and GCs. A silicon oxide cladding was applied and structured by dry and wet etching prior to the fabrication of the PPMs. The PPMs were realized with a lift-off process applied to e-beam evaporated gold ($h_{\text{Au}} = 150 \text{ nm}$). In a last step the nonlinear optical material DLD164 ($r_{33} \approx 180 \text{ pm/V}$) [30, 31] was applied by spin-coating and poled by applying a DC electric field at the glass transition temperature of the material.

Simultaneous electric field poling of several modulators at the same time is not straight forward. Single devices cannot be poled one after another. Due to heating of the chip during the poling process, electro-optic molecules in previously poled devices would relax back into a randomized order, thus the devices would lose their poling. Lattice hardening (crosslinking) of the ordered molecules [32, 33] is a solution for this problem, but the material [30] used in the presented experiments does not offer this feature. Therefore, all devices of the array have to be poled at the same time. One possibility is to contact all four MZMs individually. However, contacting eight DC probes within a few hundreds of μm is rather impractical. We therefore investigated two schemes to pole multiple devices at the same time while using only two DC probes, see Fig. 5.

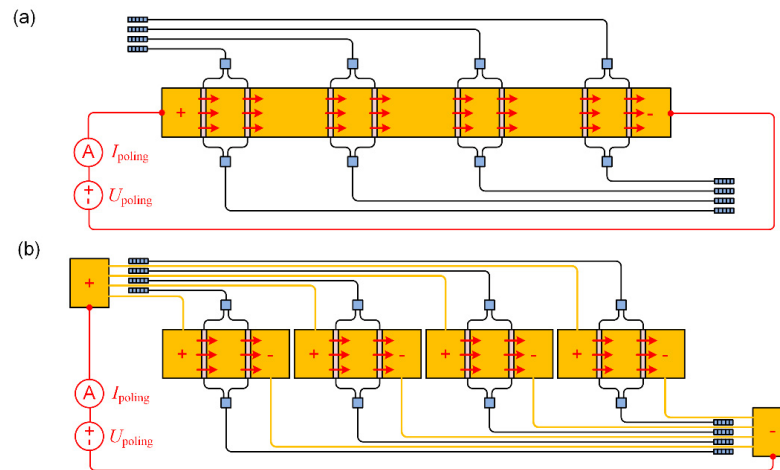


Fig. 5. Possible poling schemes. (a) Serial poling: The outer electrodes of the individual MZMs are connected, while the two most outer electrodes are contacted using DC probes to apply the poling field. The required voltage is the sum of the voltages across each component. (b) Parallel poling: The two outer electrodes of the individual MZMs are connected to poling electrodes. The voltage applied to the poling electrodes and the voltage across each component are the same and lower than for the serial scheme.

Connecting the outer electrodes of the individual modulators in series allows a serial poling, see Fig. 5(a). However, there are two major disadvantages of this scheme: First, the poling voltage required for an array of n devices is n times higher than for a single device. This can result in high voltages making special requirements for voltage source and safety precautions mandatory. Second, in case of dielectric breakdown or electrical short in one single modulator arm, the voltage across the other devices will increase significantly. This can lead to a cascade effect that destroys all modulators being poled. An alternative approach is parallel poling of the devices as illustrated in Fig. 5(b). In this scheme, the voltage applied to the poling electrodes and to each modulator is the same. Therefore, the required poling voltage is not higher than for single device poling. In case of dielectric breakdown or a short in one device, the voltage at the other modulators will not increase. The damaged device would effectively act as an electrical fuse, being destroyed completely by the high current that suddenly flows. After this process, it would appear as an open circuit, while the voltage across the other modulators would stay the same. The remaining modulators would still be poled. The disadvantage of the parallel poling scheme however is, that it requires additional design effort but does not pose a technical disadvantage. In more complex structures metal/waveguide crossings can be realized by a multiple layer process. This would allow for even easier layouts by introducing a poling layer connected to the modulators by vias. This would allow for parallel poling of all devices on a chip at the same time. Given the advantages of the lower poling voltages our decision was made in favor of the parallel poling scheme, Fig. 5(b).

4.2 Characterization

4.2.1 Static and dynamic characterization

The static characteristics of the array were studied first. The optical extinction ratios of the imbalanced interferometers were found to be in the range of 7.3...23.9 dB with insertion losses of (12.6 ± 0.7) dB. The plasmonic propagation losses within the active section were ~ 0.9 dB/ μm at a wavelength of 1550 nm. This is higher than the losses of ~ 0.5 dB/ μm as measured in our previous batch [14, 16]. Grating coupler losses contribute with 8 dB per grating.

To measure the modulation bandwidth of the individual modulators, a -3 dBm small signal RF field between 15 GHz and 70 GHz was applied to the devices. The ratio between optical carrier and modulation sidebands was measured with an optical spectrum analyzer (OSA) and normalized to 15 GHz, Fig. 6(a). This technique [34] allows to measure up to highest speeds and is only limited by the maximum frequency of the RF source (70 GHz in this case). However, the spectral resolution caused by the optical filter shape of the OSA limits the measurement to frequencies >15 GHz. Figure 6(b) depicts the normalized modulation bandwidth of all four channels. The electrical frequency response of the four channels shows no bandwidth limitation up to 70 GHz.

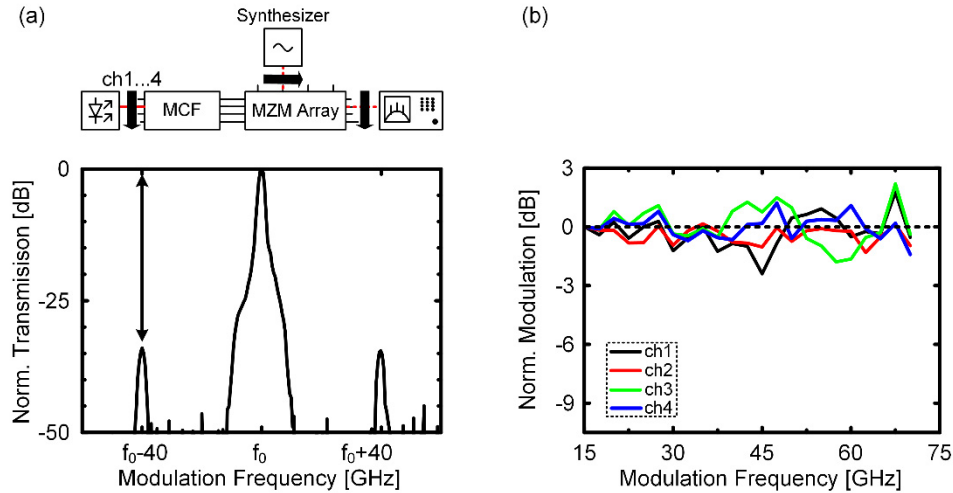


Fig. 6. RF-bandwidth characterization of the MZM array. (a) Experimental setup and measurement technique. The modulators are characterized sequentially using a sinusoidal RF waveform. The ratio of the carrier to the first modulation sideband is measured in the optical spectrum for RF-frequencies between 15 and 70 GHz (here 40 GHz). (b) Normalized modulation frequency response of all channels. The 3 dB bandwidth is above 70 GHz, thus no bandwidth limitation is expected.

4.2.2 Optical and electrical crosstalk

To investigate the optical crosstalk of the dense optical interface we fed 4 different wavelengths (1543.5 nm...1545.0 nm) through 4 different channels (ch1...ch4) of the MCF, while coupling to silicon waveguides (WGs) without MZMs. The optical output spectrum of each channel was recorded using an OSA, Fig. 7(a). Crosstalks were found to be lower than -31 dB in any instance. As an example we discuss the crosstalk into channel 2. The spectrum of channel 2 is shown in red. A main peak at 1544.0 nm is found which corresponds to the wavelength fed to channel 2. Besides, smaller peaks at the wavelengths of the neighboring channels appear in the spectrum.

The electrical crosstalk between the MZMs was investigated by applying a sinusoidal RF signal to one channel while checking for signs of modulation in the optical signals of the neighboring channels, Fig. 7(b). No modulation sidebands could be observed in a neighbor channel when any of the MZM were modulated. If there should be any crosstalk, it must be -30 dB or less, as can be inferred from the noise level of the OSA with which the measurements were performed.

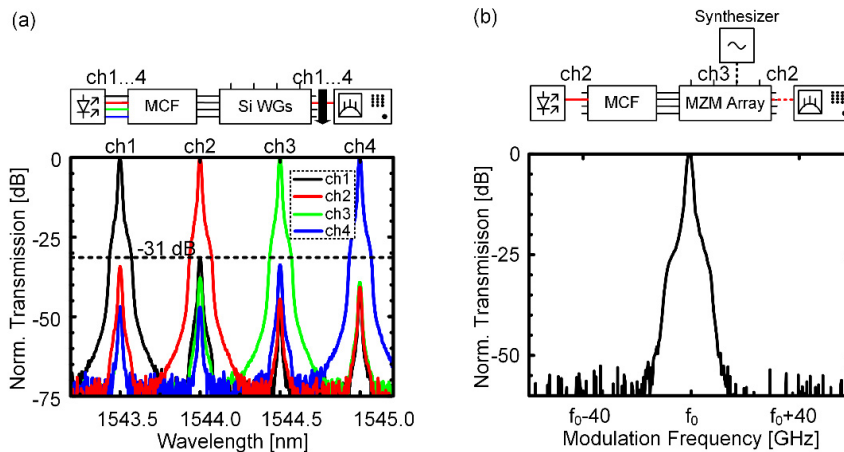


Fig. 7. Optical and electrical crosstalk characterization. (a) Optical crosstalk: Measurement setup for optical crosstalk to channel 2 and recorded optical spectrum of all channels. An optical interchannel crosstalk below -31 dB was found for all channels. The spectra were obtained by coupling four different wavelengths to the MCF. (b) Electrical crosstalk: Measurement setup for electrical crosstalk between channel 3 and channel 2 and recorded spectrum of channel 2 as an example. A sinusoidal RF signal was applied to a certain channel while checking for modulation signs of an unmodulated neighboring channel. An electrical crosstalk below -30 dB was found.

4.2.3 Data modulation experiments

The applicability of plasmonic MZMs in communication systems was verified by data modulation experiments. Data signals with binary phase shift keying (BPSK) at 36 Gbit/s were generated. The experimental setup is depicted in Fig. 8. Four CW laser sources (1549.3 nm to 1552.7 nm, $\Delta\lambda \approx 1$ nm) were coupled to the array via the MCF. Two digital-to-analog converters (72 GSa/s, 6 bit) generated uncorrelated, differential signals D_1 and D_2 (pulse shape: square-root-raised cosine, roll off $\alpha = 1$) with De Bruijn bit sequences (DBBS 2^{15}) that were amplified to $4 V_{pp}$ by RF amplifiers. $D_1, D_2, \bar{D}_1,$ and \bar{D}_2 were fed to the single ended modulators by two GSGGSG probe-arrays. The four channels were received sequentially with a standard single mode fiber in a coherent receiver. Pre-distortion and post-equalization of the electrical signal was used to mitigate the frequency dependence of the RF amplifiers and the DACs. Figure 9 depicts the measured optical eye diagrams and constellation diagrams for all four channels at 36 Gbit/s. All channels have bit error ratios (BERs) below the hard-decision FEC limit of 4.5×10^{-3} (6.7% overhead) [35]; no error was detected within the 20 million recorded bits for channel 3.

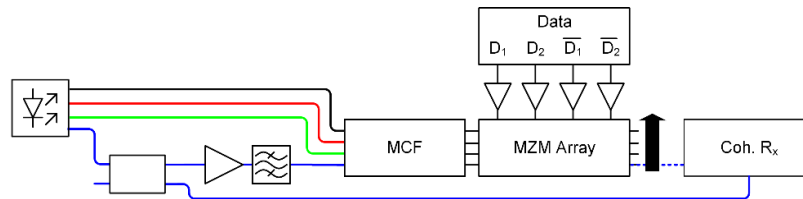


Fig. 8. Experimental setup for data modulation experiments. Four lasers with different wavelengths ($\Delta\lambda \approx 1$ nm at $\lambda \approx 1550$ nm) were coupled to a multicore fiber (MCF) and the modulator array. Four electrical data streams were fed to the modulators by two independent DACs. The laser of the channel under test was amplified before coupling to the MCF. The modulated light of the channel under test was received by a coherent receiver. The laser source of the channel under test was also used as local oscillator in the receiver.

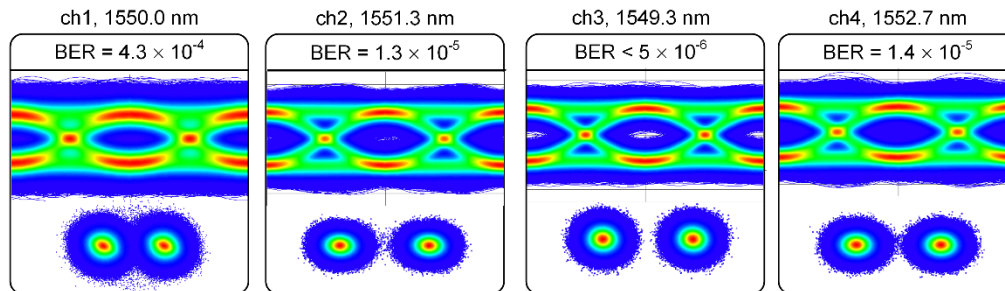


Fig. 9. Optical eye and constellation diagrams with bit error ratios (BER) of the data experiments (BPSK) at data rates of 36 Gbit/s. All four channels have a BER below the hard-decision FEC limit of 4.5×10^{-3} .

The transmitter performance can be improved further by reducing the fiber-to-chip losses. These are mainly related to fiber-chip coupling and plasmonic propagation losses. As reported in [16] plasmonic propagation losses of 0.5dB/um are feasible. Also, fiber-chip coupling loss well below 3dB/coupler have become quite common in the silicon photonics industry [36]. Reduced insertion losses will enable higher data rates at lower BERs. On a system level, the plasmonic modulators can be integrated with their driving electronics, e.g. using wire bonding, instead of RF probes. Ultimately, plasmonics and electronics shall be monolithically integrated on a chip.

5. Conclusion

A compact plasmonic transmitter concept is introduced. It consists of a dense plasmonic modulator array operating at 4×36 Gbit/s. The transmitter is connected by a $50 \mu\text{m}$ spaced optical interface using a multicore fiber. The transmitter may be used in data center applications and relates to either an operation scenario with space-division multiplexing or wavelength-division multiplexing.

Acknowledgments

This work was partly carried out at the Binnig and Rohrer Nanotechnology Center as well as in the FIRST clean-room facility at the ETH Zurich. The EU-project NAVOLCHI (288869), the EU funded ERC PLASILOR (670478) and the National Science Foundation Grant (DMR-1303080) are acknowledged for partial funding of this project. The authors thank Ueli Koch, Hans-Rudolf Benedickter, Martin Lanz, Claudio Maccio and Aldo Rossi.